Symmetry of the Magnetic Orbitals and Exchange Interaction in $Cu^{II}Fe^{III}$ and $Cu^{II}Cr^{III}$ Heterobinuclear Complexes. Crystal Structure of $CuFe[(fsa)_2en]Cl(H_2O)(CH_3OH)\cdot CH_3OH$

Yves Journaux,[†] Olivier Kahn,*[†] Jacqueline Zarembowitch,[†] Jean Galy,*[‡] and Joël Jaud[‡]

Contribution from the Laboratoire de Spectrochimie des Elēments de Transition, ERA 672, Universitē de Paris Sud, 91405 Orsay, France, and the Laboratoire de Chimie de Coordination, Associē à l'Universitē Paul Sabatier, 31030 Toulouse, France. *Received December 6, 1982*

Abstract: The two heterobinuclear complexes $CuFe[(fsa)_2en]Cl(H_2O)(CH_3OH)\cdot CH_3OH$ and $[CuCr[(fsa)_2en](H_2O)_2]Cl\cdot 3H_2O$, noted $Cu^{II}Fe^{III}$ and $Cu^{II}Cr^{III}$, respectively, have been synthesized. $[(fsa)_2en]^{4-}$ is the binucleating ligand derived from the Schiff base *N,N'*-bis(2-hydroxy-3-carboxybenzylidene)-1,2-diaminoethane. The crystal structure of $Cu^{II}Fe^{III}$ has been solved at room temperature. It crystallizes in the monoclinic system, space group $P2_1/c$. The lattice constants are a = 10.619 (6) Å, b = 11.698 (4) Å, c = 18.429 (9) Å, β = 101.6(3)° with Z = 4. The structure is made of heterobinuclear units, in which the copper is fivefold coordinated to two nitrogens, two phenolic oxygens, and a methanol molecule, and the iron is hexacoordinated to two phenolic oxygens, two carboxylic oxygens, a chlorine atom, and a water molecule. The molecular structure of $Cu^{II}Cr^{III}$ has been derived from chemical considerations and infrared data, with the copper occupying the N_2O_2-inside site and the chromium the O_2O_2-outside site with two water molecules in apical position to achieve the octahedral surrounding. The magnetic properties of the two complexes have been studied in the 4.2–300 K temperature range. They reveal that for both $Cu^{II}Fe^{III}$ and $Cu^{II}Cr^{III}$ the ground state is a spin quintet (S = 2). In $Cu^{II}Fe^{III}$, this state arises from an antiferromagnetic interaction, $^2B_1 \leftrightarrow {}^6A_1$, the main component being $J_{b_1b_1}$ between magnetic orbitals of b_1 symmetry (referring to C_{2v} site group). In $Cu^{II}Cr^{III}$, the ground state arises from a ferromagnetic interaction, $^2B_1 \leftrightarrow {}^4B_1$, due to the strict orthogonality of the b_1 magnetic orbital around the copper and the a_1, a_2, and b_2 magnetic orbitals around the chromium. Quantitatively, the exchange parameters of the $-J_{AB}S_A\cdot S_B$ exchange Hamiltonian were found as $J_{CuFe} = -78$ cm^{-1} and $J_{CuCr} = +105$ cm^{-1}. In both cases, the ground state undergoes a large zero-field splitting with $|D| \simeq 8$ cm^{-1} in $Cu^{II}Fe^{III}$ and 5 cm^{-1} in $Cu^{II}Cr^{III}$. Finally, the sign and magnitude of the $J_{\mu\nu}$ components involving pairs of magnetic orbitals are discussed from considerations of overlap densities $\rho_{\mu\nu}$.

In the fifties, solid-state chemists and physicists such as Goodenough[1] and Kanamori[2] proposed empirical rules to predict the nature of the exchange interaction between M and M' metallic centers bridged by X monoatomic ligands.[3] These rules, of which a good presentation has been given by Ginsberg,[4] are based on the examination of the exchange pathway along each M–X–M' linkage. Such an approach gave interesting results concerning the solid-state materials. In particular, it permitted putting into evidence situations where a ferromagnetic interaction could be expected. This is the case, for instance, for the interaction at 90° between *xy*-type metallic orbitals,[4] as shown in **1**. With the usual

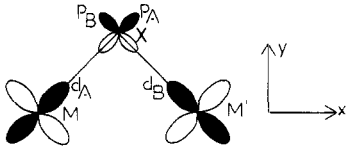

1

notations,[4] one may write the exchange pathway as $d_A \| p_A \perp p_B \| d_B$, which actually corresponds to a ferromagnetic coupling. This approach, however, has a severe defect. It does not take into account the actual symmetry of the system. So, when there are several bridging atoms, it ignores the phase relations between the different M–X–M' linkages.[5-6] Using a terminology introduced in a previous paper,[5] we may say that the Goodenough–Kanamori rules explain the ferromagnetic coupling when this is due to the *accidental orthogonality* of the *magnetic orbitals* but not when this is due to the *strict orthogonality*. Examples of accidental and strict orthogonalities are given in **2**, where we represented the ϕ_A and ϕ_B magnetic orbitals at the top and the overlap densities $\rho(i) = \phi_A(i)\phi_B(i)$ at the bottom. The first column refers to a $Cu^{II}Cu^{II}$ pair and the second to a $Cu^{II}VO^{II}$ pair.[7] As was already noticed,[5] ignoring the phases in the case of strict orthogonality, we could obtain the erroneous conclusion that along each M–X–M'

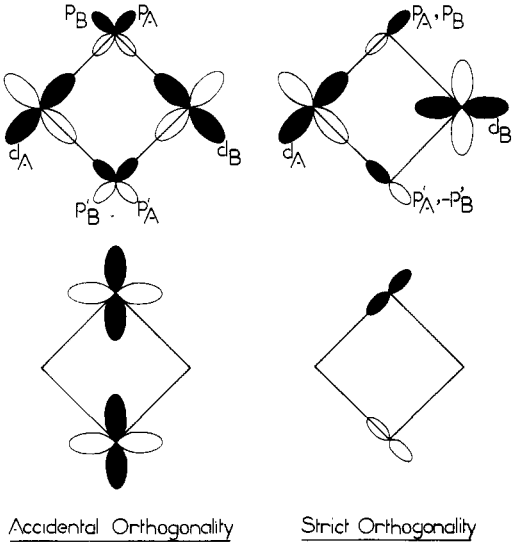

2

linkage the $d_A \| p \| d_B$ pathway gives antiparallel coupling, hence that the overall interaction should be antiferromagnetic. The accidental orthogonality can be destroyed by a very small variation of the bridging angles, whereas in the case of strict orthogonality, such a variation has as only consequence to modify slightly the magnitude of the ferromagnetic interaction.[7] Therefore, to design a ferromagnetic interaction between two metal ions, the strategy

[†] Universitē de Paris Sud.
[‡] Universitē Paul Sabatier.

(1) Goodenough, J. B. *Phys. Rev.* **1955**, *100*, 564–573; *J. Phys. Chem. Solids* **1958**, *6*, 287–297.
(2) Kanamori, J. *J. Phys. Chem. Solids* **1959**, *10*, 87–98.
(3) Anderson, P. W. In "Magnetism"; Rado, G. T., Suhl, H., Eds.; Academic Press: New York, 1963; Vol. 1, Chapter 2.
(4) Ginsberg, A. P. *Inorg. Chim. Acta, Rev.* **1971**, *5*, 45–68.
(5) Kahn, O.; Galy, J.; Journaux, Y.; Jaud, J.; Morgenstern-Badarau, I. *J. Am. Chem. Soc.* **1982**, *104*, 2165–2176.
(6) Eremin, M. V.; Rakitin, Yu V. *J. Phys. C* **1982**, *15*, L 259–L 261.
(7) Kahn, O.; Charlot, M. F. *Nouv. J. Chim.* **1980**, *4*, 567–576.

0002-7863/83/1505-7585$01.50/0

based on the concept of strict orthogonality is by far the most efficient.

Although out of the scope of this paper, we can mention here another defect of the Goodenough–Kanamori rules: they are apparently inapplicable for systems with extended bridging ligands.

In this paper, we propose to prove the heuristic character of the models of the exchange interaction which lean on the symmetry properties of the polymetallic entities in their whole and therefore which take into account the phase relations between the bridges. This work deals with molecular entities. Nevertheless, we hope that it will be of interest for the solid-state chemists and physicists dealing with the magnetic properties of the condensed phases. For that, we describe two new heterobinuclear complexes containing the $Cu^{II}Fe^{III}$ and $Cu^{II}Cr^{III}$ pairs, respectively. These two complexes have the same ground state, namely a spin quintet state. For the former complex, the nature of this ground state results from an intramolecular antiferromagnetic interaction; for the latter, it results from a ferromagnetic interaction due to the strict orthogonality of the magnetic orbitals. We also describe the crystal structure of the $Cu^{II}Fe^{III}$ complex. Two preliminary communications were devoted to these compounds.[8,9] The quantitative values of the exchange parameters given in this paper are somewhat different from those already published. Indeed, in the preliminary communications, we had not taken into account the large zero-field splitting of the ground state. The investigation of the magnetic properties of a $Ni^{II}Fe^{III}$ complex where only the Fe^{III} ion is magnetic showed to us the importance of the local anisotropy of the Fe^{III} ion. That is why the study of this complex is included in this paper.

Experimental Section

Syntheses. $CuFe[(fsa)_2en]Cl(H_2O)(CH_3OH)\cdot CH_3OH$, noted hereafter $Cu^{II}Fe^{III}$, was synthesized as follows: first, the sodium salt of $CuH_2[(fsa)_2en]\cdot{}^1/_2H_2O$ was prepared by stirring together 2×10^{-4} mol of $CuH_2[(fsa)_2en]\cdot{}^1/_2H_2O$[10] and 4×10^{-4} mol of NaOH in 40 mL of methanol. The solution was filtered, and then a solution of 2×10^{-4} mol of $FeCl_3\cdot 6H_2O$ in 10 mL of methanol was added. Well-shaped dark-red single crystals were obtained by slow evaporation. Anal. Calcd for $C_{20}H_{22}N_2O_9ClCuFe$: C, 40.77; H, 3.76; N, 4.75; Cl, 6.02. Found: C, 40.78; H, 3.70; N, 4.95; Cl, 6.25.

$[CuCr[(fsa)_2en](H_2O)_2]Cl\cdot 3H_2O$, noted hereafter $Cu^{II}Cr^{III}$, was synthesized by stirring a solution of 2×10^{-4} mol of $CrCl_3\cdot 6H_2O$ in 50 mL of methanol with a suspension of 2×10^{-4} mol of $CuH_2[(fsa)_2en]\cdot{}^1/_2H_2O$. After 3 weeks, the mixture becomes limpid and apparently well-shaped, small dark-blue single crystals were obtained by slow evaporation. Anal. Calcd for $C_{18}H_{22}N_2O_9ClCuCr$: C, 36.44; H, 3.74; N, 4.72; Cl 5.97; Cu, 10.71; Cr 8.76. Found: C, 36.72; H, 3.84; N, 4.54; Cl, 5.88; Cu, 10.3; Cr, 8.2.

$NiFe[(fsa)_2en]Cl(CH_3OH)\cdot H_2O$ was synthesized as follows: first, the lithium salt of $FeH_2[(fsa)_2en]Cl(CH_3OH)\cdot H_2O$ was prepared by stirring together 2×10^{-4} mol of $FeH_2[(fsa)_2en]Cl(CH_3OH)\cdot H_2O$[11] and 4×10^{-4} mol of LiOH in 40 mL of methanol. The solution was filtered. Then a solution of 2×10^{-4} mol of $NiCl_2\cdot 6H_2O$ in 50 mL of methanol was added and the mixture was heated at reflux during 15 min. The compound precipitates as a brown polycrystalline powder. Anal. Calcd for $C_{19}H_{20}N_2O_8ClNiFe$: C, 41.32; H, 3.28; N, 5.07; Cl, 6.42. Found: C, 41.27; H, 3.22; N, 5.00; Cl, 6.34. Under prolonged vacuum, the compound loses its water molecule.

X-ray Analysis. Structure Determination. The preliminary X-ray studies were conducted by photographic methods using a Weissenberg Camera (Ni-filtered Cu Kα radiation). The crystal system, monoclinic, the approximation unit cell parameters, and the space group, $P2_1/c$, were derived from these photographic data. Intensity data were collected at room temperature on a CAD 4 Enraf-Nonius PDP8/M computer-controlled single-crystal diffractometer. All the information concerning crystallographic data collections and results is summarized in Table I. The unit cell parameters have been refined by optimizing the settings of 25 reflections. The intensity of the utilized reflections [$I > \sigma(I)$] was corrected for Lorentz and polarization factors. After azimuthal measurements of the intensity of some *hkl* reflections, it was decided not to apply absorption corrections ($\mu r \simeq 0.3$). Atomic scattering factors of Cromer and Waber[12] for the non-hydrogen atoms and of Stewart, Davidson, and Simpson[13] for the spherical hydrogen atoms were used. Real and imaginary dispersion corrections given by Cromer were applied for copper, iron, and chlorine atoms.[14]

The structure was solved after deconvolution of Patterson function, which gave the coordinates of the heavy atoms and their nearest-neighbor oxygen and nitrogen atoms. From Fourier synthesis, it was possible to locate the remaining oxygen and carbon atoms. The structure was then refined by full-matrix least-squares techniques. Difference Fourier maps and a priori calculations made it possible for the positions of the hydrogen atoms to be determined. All non-hydrogen atoms were then allowed to refine with anisotropic thermal parameters and a fixed isotropic thermal parameter of $B_H = 1.2B_{eq}(C)$ Å^2 was used for hydrogen atoms. ($B_{eq}(C)$ is the isotropic equivalent factor of the carbon to which the hydrogen is bound: $B_{eq}(C) = {}^4/_3\sum_{i,j}[(\vec{a}_i\vec{a}_j)\beta_{ij}]$. The last difference Fourier map did not show us any peak greater than 0.3 e Å^{-3}. The R factor is then 0.074.

Magnetic measurements were carried out on polycrystalline samples weighing about 5 mg in the temperature range 4.2–300 K with a Faraday type magnetometer equipped with a continuous-flow cyrostat. The applied magnetic field were about 0.2 T. The independence of the susceptibility against the magnetic field was checked at room temperature. Mercurytetrakis(thiocyanato)cobaltate was used as a susceptibility standard. The uncertainty on the temperature is about 0.1 K, and on the susceptibility about 100×10^{-6} cm^3 mol^{-1}. It follows that the uncertainty on $\chi_M T$ is about 0.03 cm^3 mol^{-1} K. For each compound, the number of measured points is around 150. The diamagnetism was estimated as -230×10^{-6} cm^3 mol^{-1} for the $Cu^{II}Fe^{III}$ and $Ni^{II}Fe^{III}$ complexes and -280×10^{-6} cm^3 mol^{-1} for the $Cu^{II}Cr^{III}$ complex.

Structure of the $Cu^{II}Fe^{III}$, $Cu^{II}Cr^{III}$, and $Ni^{II}Fe^{III}$ Compounds

Crystal Structure of $CuFe[(fsa)_2en]Cl(H_2O)(CH_3OH)\cdot CH_3OH$. Atomic coordinates and anisotropic temperature factors are given in Table II. The main interatomic distances, bond lengths, and angles are listed in Table III. The asymmetric unit cell contains one $CuFe[(fsa)_2en]Cl(H_2O)(CH_3OH)$ molecule and one noncoordinated methanol molecule. The perspective view of these two molecules is given in Figure 1, with the already described atom labeling[5] completed for the extra atoms.

The structural data concerning the ligand part of the complex are in good agreement with the previous studies dealing with compounds of the same family[5,15–17] and do not warrant any additional comment. The copper atom occupying the inside site shows a fivefold coordination in the form of a square pyramid with the two nitrogen atoms N(5) and N(6) and the two phenolic oxygen atoms O(1) and O(2) in the basal plane and the oxygen atom O(6) of a methanol molecule at the apex. The Cu–O(6) bond length is 2.277 (7) Å, and the copper atom is pulled out of the mean plane O(1)O(2)N(5)N(6) by 0.21 (1) Å.

In the outside site, the iron atom is sixfold coordinated, the phenolic and carboxylic oxygen atoms, O(1)O(2)O(3)O(4), delimiting the equatorial plane of an octahedron the apexes of which are being occupied by a water molecule and a chlorine atom, respectively. This octahedron is rather distorted in spite of classical Fe–OH_2, Fe–O, and Fe–Cl bond lengths; the iron atom is pulled out of the equatorial plane by 0.14 (1) Å in the direction of the chlorine atom. The methanol molecule bound to copper and this chlorine atom are situated in the trans position with regard to the average plane of the molecule; they are apparently too big to occupy neighbor positions.

The plane containing copper, iron, and chlorine is almost a bisector plane for the molecule. Nevertheless, the steric repulsion between the methanol and water molecules pushes O(CH_3OH) and O(H_2O) apart from this plane.

(8) Jaud, J.; Journaux, Y.; Galy, J.; Kahn, O. *Nouv. J. Chim.* **1980**, *4*, 629–630.
(9) Journaux, Y.; Kahn, O.; Coudanne, H. *Angew. Chem., Int. Ed. Engl.* **1982**, *21*, 624–625.
(10) Tanaka, M.; Kitaoka, M.; Okawa, H.; Kida, S. *Bull. Chem. Soc. Jpn.* **1976**, *49*, 2469–2473.
(11) Zarembowitch, J.; Kahn, O.; Jaud, J.; Galy, J. *Inorg. Chim. Acta* **1982**, *64*, L 35–L 36.
(12) Cromer, D. T.; Waber, J. T. *Acta. Crystallogr.* **1965**, *18*, 104–109.
(13) Stewart, R. F.; Davidson, E. R.; Simpson, W. T. *J. Chem. Phys.* **1965**, *42*, 3175–3187.
(14) Cromer, D. T. *J. Chem. Phys.* **1969**, *50*, 4857–4859.
(15) Morgenstern-Badarau, I.; Rerat, M.; Kahn, O.; Jaud, J.; Galy, J. *Inorg. Chem.* **1982**, *21*, 3050–3059 and references therein.
(16) Mikuriya, M.; Okawa, H.; Kida, S.; Ueda, I. *Bull. Chem. Soc. Jpn.* **1978**, *51*, 2920–2923.
(17) Beale, J. P.; Cunningham, J. A.; Phillips, D. J. *Inorg. Chim. Acta* **1979**, *33*, 113–118.

Table I. Information Concerning Crystallographic Data Collection

1. Crystallographic and Physical Data	
formula	$CuFeO_9N_2C_{20}H_{22}Cl$
crystal system	monoclinic
a, A	10.619 (6)
b, A	11.698 (4)
c, A	18.429 (9)
β, deg	101.6 (3)
M_r	589.25
space group	$P2_1/c$
V, A^3	2242
Z	4
$F(000)$	1968
ρ_{exptl}, g/cm^3	1.73 (3)
ρ_X	1.746
absorption factor, cm^{-1}	18.2 (Mo Kα)
morphology: cm (average radius)	0.015
little regular block	
2. Data Collection	
temp, K	293
radiation	Mo Kα
monochromatisation: monochromator	
graphite λ Kα, A	0.71069
crystal-detector distance, mm	207
detector window: height,[a] mm	4
width,[a] mm	4
takeoff angle,[a] deg	4
scan mode	$\theta/2\theta$
maximum Bragg angle, deg	31
scan angle for ω angle	0.85 + 0.347 tan θ
values determining the scan-speed	
Sigpre[a]	0.800
Sigma[a]	0.018
Vpre[a], deg/mm	7
T_{max}[a], s	80
controls	
reflections	
intensity periodicity, 3600 s	$0\bar{6}0$, $00\bar{1}0$, $5\bar{3}\bar{4}$
orientation after 100 reflections	434, 400, 326
3. Conditions for Refinement	
reflections for the refinement of the cell dimensions	25
recorded reflections	4308
independent reflections: obsd	2904
utilized reflections $I > \sigma(I)$	2713
refined parameters	307
reliability factors	
$R = \Sigma \lvert kF_o - \lvert F_c \rvert \rvert / \Sigma kF_o$	0.0748
$R_w = [\Sigma(kF_o - \lvert F_c \rvert)^2 / \Sigma wk^2F_o^2]^{1/2}$	0.0739

[a] Mosset, A.; Bonnet, J. J.; Galy, J. *Acta Crystallogr., Sect. B* 1977, *B33*, 2639-2643.

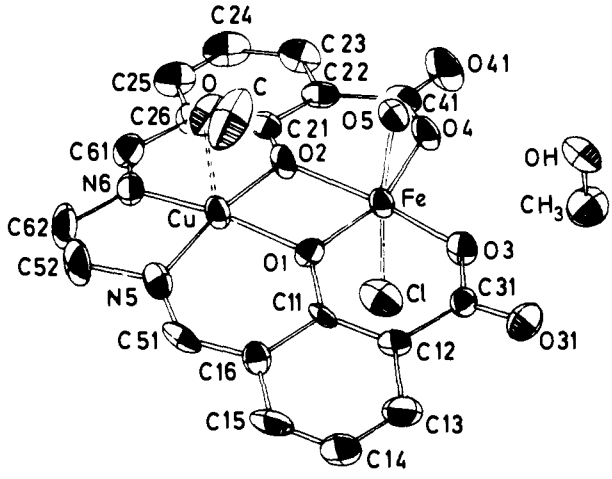

Figure 1. Perspective view of $CuFe(fsa)_2enCl(H_2O)(CH_3OH)\cdot CH_3OH$.

The O(1)–O(2) distance, as in all the binuclear complexes,[15] is shortened due to metal–metal repulsion with regard to the mononuclear complex containing only a copper atom in the inside site,[18] 2.538 (8) Å and 2.744 (9) Å, respectively. The CuO(1)Fe and CuO(2)Fe bridging angles are equal to 100.7 (3)° and 99.4 (3)°, respectively. The O(3)–O(4) distance, 3.108 (9) Å, is very close to those already determined in complexes having an octahedral environment for the outside site.[15]

The molecular packing does not exhibit special features. The second methanol molecule, unrelated with the complex, can be regarded as a molecule of crystallization.

Structure of $[CuCr[(fsa)_2en](H_2O)_2]Cl\cdot 3H_2O$. In spite of many attempts, we were unable to obtain single crystals of the $Cu^{II}Cr^{III}$ complex suitable for X-ray investigation. Although very small, most of the crystals appeared well shaped. However, in their bulk, they were "disorganized". This could be due to the loss of noncoordinated water molecules. Cl^- can be easily replaced by noncoordinating counterions like PF_6^-, without any modification of the infrared spectrum (except, of course, the appearance of the T_{1u} vibrations of PF_6^-), suggesting strongly that Cr^{III} achieves its octahedral surrounding by fixing two water molecules in apical positions, as shown in **3**.

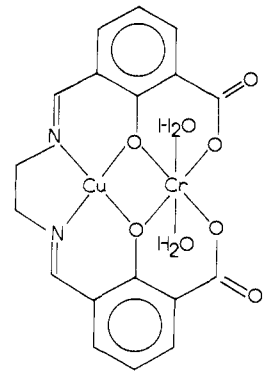

3

Structure of $NiFe[(fsa)_2en]Cl(CH_3OH)\cdot H_2O$. The occupation of the sites in the $Ni^{II}Fe^{III}$ complex is unambiguously determined by the magnetic properties, characteristic of an uncoupled high-spin Fe^{III} ion (vide infra). Therefore, the Ni^{II} ion is located in the planar N_2O_2– inside site and the Fe^{III} in the oustide site. This result is obtained although the starting material was $FeH_2[(fsa)_2en]Cl(CH_3OH)\cdot H_2O$ with Fe^{III} in the inside site.[11] It had already been shown that Fe^{III} can easily move from one site to the other one.[11] In fact, our complex is identical with the one prepared by Okawa et al.[19] by reaction of $FeCl_3\cdot 6H_2O$ on $NiH_2[(fsa)_2en]$. The insolubility of the $Ni^{II}Fe^{III}$ complex in the protic solvents indicates that the chlorine is bound to the iron, the coordinance six being likely achieved by the methanol molecule, which is less labile than the water molecule. The structure is schematized in **4**.

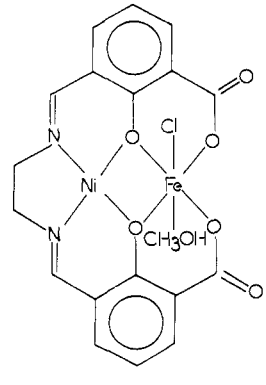

4

Magnetic Properties. The magnetic properties of $Cu^{II}Fe^{III}$ and $Cu^{II}Cr^{III}$ are given together in Figure 2 in the form of $\chi_M T$ vs. T plot, χ_M being the molecular magnetic susceptibility and T the

(18) Unpublished result.
(19) Okawa, H.; Kanda, W.; Kida, S. *Chem. Lett.* **1980**, 1281–1284.

Table II. Positional and Thermal Parameters for the Atoms of $CuFeClN_2O_9C_{20}H_{20}$[a]

atom	x	y	z	b_{11} or b, A^2	b_{22}, A	b_{33}	b_{12}	b_{13}	b_{23}
Cu(1)	−0.2380 (1)	0.2715 (1)	0.27820 (7)	7.7 (2)	2.92 (9)	2.11 (5)	0.13 (10)	0.44 (6)	0.73 (6)
Fe(1)	−0.2121 (1)	0.0867 (1)	0.39571 (8)	6.0 (1)	2.35 (9)	1.71 (5)	−0.2 (1)	0.17 (6)	0.19 (6)
Cl(1)	−0.4138 (3)	0.1138 (2)	0.4210 (2)	7.1 (3)	5.9 (2)	4.6 (1)	−0.2 (2)	1.8 (2)	0.1 (1)
O(1)	−0.2676 (7)	0.1095 (5)	0.2860 (4)	9.8 (8)	1.6 (4)	2.1 (2)	−0.5 (5)	0.4 (4)	0.5 (3)
O(2)	−0.1760 (6)	0.2569 (5)	0.3834 (3)	8.2 (8)	3.0 (5)	1.5 (2)	−1.2 (5)	1.0 (3)	−0.5 (3)
O(5)	−0.2341 (7)	−0.0745 (5)	0.3773 (4)	9.0 (8)	2.0 (5)	2.5 (3)	0.1 (5)	0.1 (4)	0.3 (3)
O(4)	−0.1318 (7)	0.1050 (5)	0.4992 (4)	10.4 (9)	2.1 (5)	2.1 (3)	−1.0 (5)	0.2 (4)	−0.3 (5)
N(6)	−0.2399 (9)	0.4344 (7)	0.2801 (5)	10.0 (1)	3.5 (7)	2.8 (4)	0.3 (7)	1.3 (5)	1.0 (4)
N(5)	−0.3379 (8)	0.2854 (7)	0.1799 (5)	6.5 (9)	4.9 (7)	1.8 (3)	0.5 (7)	0.6 (4)	0.7 (4)
O(31)	−0.3215 (8)	−0.2353 (6)	0.3315 (5)	15.0 (1)	2.4 (5)	4.3 (4)	−0.6 (6)	−0.3 (5)	−0.1 (4)
O(41)	−0.0548 (8)	0.1791 (7)	0.6065 (4)	13.0 (1)	8.9 (8)	1.6 (3)	1.5 (8)	−0.1 (4)	−0.6 (4)
O	−0.0186 (6)	0.0542 (5)	0.3828 (4)	6.4 (7)	4.1 (5)	2.5 (3)	0.6 (5)	0.8 (3)	0.5 (3)
C(11)	−0.3378 (9)	0.0399 (8)	0.2353 (6)	3.4 (9)	4.2 (7)	2.2 (4)	0.3 (7)	0.5 (5)	−0.2 (4)
C(12)	−0.3543 (9)	−0.0755 (8)	0.2513 (6)	6.0 (1)	3.7 (7)	2.5 (4)	−0.8 (7)	1.0 (5)	−1.3 (5)
C(13)	−0.424 (1)	−0.1463 (9)	0.1962 (7)	6.0 (1)	5.3 (9)	3.5 (5)	−1.2 (8)	0.5 (6)	−1.1 (5)
C(14)	−0.481 (1)	−0.1025 (10)	0.1272 (7)	10.0 (1)	6.0 (1)	3.3 (5)	−3.0 (10)	0.2 (6)	−2.9 (6)
C(15)	−0.468 (1)	0.009 (1)	0.1121 (6)	7.0 (1)	8.0 (1)	2.4 (4)	−0.4 (10)	−0.6 (6)	−1.7 (6)
C(16)	−0.3969 (10)	0.0853 (9)	0.1649 (6)	7.0 (1)	6.0 (9)	2.0 (4)	1.8 (9)	0.5 (5)	0.3 (5)
C(21)	−0.1687 (9)	0.3346 (7)	0.4360 (6)	5.3 (10)	1.2 (6)	2.5 (4)	0.9 (6)	1.0 (5)	0.3 (4)
C(22)	−0.1363 (9)	0.3108 (7)	0.5122 (6)	6.0 (1)	2.1 (6)	2.1 (4)	−1.2 (6)	0.7 (5)	−0.9 (4)
C(23)	−0.130 (1)	0.4016 (10)	0.5640 (6)	9.0 (1)	6.6 (10)	2.8 (4)	1.6 (10)	0.9 (6)	−0.9 (6)
C(24)	−0.155 (1)	0.5114 (10)	0.5418 (7)	14.0 (2)	4.8 (9)	2.7 (5)	0.8 (10)	0.4 (7)	−1.5 (5)
C(25)	−0.181 (1)	0.5354 (9)	0.4688 (7)	11.0 (1)	3.8 (8)	4.1 (5)	1.8 (9)	2.2 (7)	−1.2 (6)
C(26)	−0.1904 (9)	0.4566 (8)	0.4131 (6)	7.0 (1)	3.5 (7)	2.2 (4)	−0.5 (7)	0.6 (5)	0.4 (4)
C(31)	−0.3011 (10)	−0.1352 (9)	0.3250 (6)	6.0 (1)	4.5 (8)	3.0 (4)	1.1 (8)	1.4 (5)	−0.1 (5)
C(41)	−0.1060 (9)	0.1932 (8)	0.5409 (5)	4.4 (10)	4.4 (7)	1.5 (3)	0.5 (7)	0.1 (5)	0.2 (4)
C(51)	−0.397 (1)	0.202 (1)	0.1415 (6)	8.0 (1)	8.0 (1)	2.1 (4)	1.6 (9)	1.5 (6)	0.9 (5)
C(61)	−0.2225 (10)	0.4954 (7)	0.3386 (7)	7.0 (1)	0.8 (6)	4.1 (5)	−0.2 (7)	1.0 (6)	−0.4 (5)
C(62)	−0.272 (2)	0.4823 (9)	0.2041 (7)	25.0 (2)	3.0 (8)	3.0 (5)	1.0 (1)	1.4 (9)	1.6 (5)
C(52)	−0.353 (1)	0.403 (1)	0.1541 (6)	17.0 (2)	5.5 (10)	2.3 (4)	0.0 (1)	0.9 (7)	1.8 (6)
O(5)	−0.1609 (6)	−0.1789 (6)	0.5184 (4)	5.8 (8)	4.3 (5)	4.0 (3)	0.4 (5)	0.7 (4)	0.2 (4)
O(6)	−0.0456 (7)	0.2487 (7)	0.2434 (4)	9.2 (9)	9.2 (8)	2.2 (3)	−1.7 (7)	1.1 (4)	0.2 (4)
C(7)	−0.285 (1)	−0.179 (1)	0.5345 (7)	8.0 (1)	10.0 (1)	3.3 (5)	0.0 (1)	0.9 (6)	−0.1 (7)
C(8)	0.064 (2)	0.288 (2)	0.2841 (8)	16.0 (2)	20.0 (2)	2.9 (5)	−3.0 (2)	0.9 (9)	1.7 (9)
H(113)	−0.435	−0.227	0.206	4.1					
H(114)	−0.530	−0.155	0.089	4.8					
H(115)	−0.510	0.039	0.063	4.4					
H(123)	−0.110	0.381	0.617	4.3					
H(124)	−0.153	0.573	0.579	4.9					
H(125)	−0.197	0.617	0.454	4.6					
H(152)	−0.338	0.408	0.104	5.2					
H(252)	−0.445	0.426	0.151	5.2					
H(162)	−0.313	0.556	0.204	5.4					
H(262)	−0.192	0.491	0.185	5.4					
H(161)	−0.233	0.579	0.331	3.7					
H(151)	−0.445	0.220	0.091	4.0					
H(15)	−0.120	−1/4	0.520	4.2					
H(17)	−0.310	−0.260	0.540	5.2					
H(27)	−0.350	−0.150	0.490	5.2					
H(37)	−0.280	−0.130	0.580	5.2					
H(16)	0.070	0.330	0.340	4.6					
H(18)	0.110	0.230	0.320	5.8					
H(28)	0.046	0.355	0.316	5.8					
H(38)	1/8	0.315	0.255	5.8					

[a] Estimated standard deviations in the least significant figure(s) are given in parentheses in this and all subsequent tables. The form of the anisotropic thermal ellipsoid is $\exp -(b_{11}h^2 + b_{22}k^2 + b_{33}l^2 + 2b_{12}hk + 2b_{13}hl + 2b_{23}kl)$. The quantities given in the table are the thermal coefficients $\times 10^3$.

temperature. One immediately notices that, in the range 300–60 K, the two complexes behave in an opposite way. When the temperature is decreased from room temperature, $\chi_M T$ decreases for $Cu^{II}Fe^{III}$ and increases for $Cu^{II}Cr^{III}$. The curve for $Cu^{II}Fe^{III}$ exhibits a plateau around 60 K with $\chi_M T = 3.03$ cm^3 mol^{-1} K whereas the curve for $Cu^{II}Cr^{III}$ has a maximum around 60 K with almost the same value of $\chi_M T$, namely 2.93 cm^3 mol^{-1} K. Below 50 K, for both complexes, $\chi_M T$ decreases upon cooling to the very low temperatures.

The qualitative interpretation of the two curves is straightforward. The site symmetry for both metallic ions in $Cu^{II}Cr^{III}$ and the whole molecular symmetry are very close to C_{2v} (see **3**). In $Cu^{II}Fe^{III}$, these symmetries are actually C_s but not too far from C_{2v} so that we shall use the irreducible representations of C_{2v} to label the energy levels in both complexes. The implications of this approximation for $Cu^{II}Fe^{III}$ will be discussed in the next section. The single-ion ground state for Cu^{II} with a planar surrounding is $^2B_1$. For high-spin Fe^{III} it is $^6A_1$, and for Cr^{III} it is $^4B_1$. In $Cu^{II}Fe^{III}$, the interaction $^2B_1 \leftrightarrow {}^6A_1$ leads to the two low-lying states $^5B_1$ and $^7B_1$. The decrease of $\chi_M T$ upon cooling down shows that $^5B_1$ is lower in energy. Therefore, the interaction is of antiferromagnetic nature. In $Cu^{II}Cr^{III}$, the interaction $^2B_1 \leftrightarrow {}^4B_1$ leads to the two low-lying states $^5A_1$ and $^3A_1$. The increase of $\chi_M T$ upon cooling down shows that $^5A_1$ is lower in energy. Thus, the interaction is of ferromagnetic nature. The most noteworthy point is that *in both complexes, the ground state is a spin quintet. In $Cu^{II}Fe^{III}$, this state arises from an antiferromagnetic interaction; in $Cu^{II}Cr^{III}$, it arises from a ferromagnetic interaction.*

The magnetic behaviors below 50 K are more difficult to interpret unambiguously. They may result from antiferromagnetic intermolecular interactions and/or large zero-field splittings of the quintet ground states. Two facts suggest that the zero-field splitting plays a dominant role: (i) if we replace Cl^- in $Cu^{II}Cr^{III}$

Table III. Main Bond Lengths and Bond Angles for $CuFe[(fsa)_2en]Cl(H_2O)(CH_3OH)\cdot CH_3OH$

Cu(1)-O(1)	1.931 (6)	Cu(1)-O(2)	1.926 (7)
Cu(1)-N(5)	1.914 (8)	Cu(1)-N(6)	1.907 (8)
Cu(1)-O(6)	2.277 (7)	Fe(1)-O(1)	2.006 (7)
Fe(1)-O(2)	2.049 (6)	Fe(1)-O(3)	1.922 (6)
Fe(1)-O(4)	1.939 (7)	Fe(1)-O(5)	2.150 (7)
Fe(1)-Cl(1)	2.303 (3)	O(1)-C(11)	1.35 (1)
O(2)-C(21)	1.32 (1)	O(3)-C(31)	1.29 (1)
O(4)-C(41)	1.28 (1)	N(5)-C(51)	1.29 (1)
N(5)-C(52)	1.46 (1)	N(6)-C(61)	1.27 (1)
N(6)-C(62)	1.48 (1)	O(31)-C(31)	1.20 (1)
O(41)-C(41)	1.23 (1)	C(11)-C(12)	1.40 (1)
C(11)-C(16)	1.43 (1)	C(12)-C(13)	1.40 (1)
C(12)-C(31)	1.53 (1)	C(13)-C(14)	1.39 (1)
C(14)-C(15)	1.34 (1)	C(15)-C(16)	1.42 (1)
C(16)-C(51)	1.43 (1)	C(21)-C(22)	1.41 (1)
C(21)-C(26)	1.49 (1)	C(22)-C(23)	1.42 (1)
C(22)-C(41)	1.48 (1)	C(23)-C(24)	1.36 (1)
C(24)-C(25)	1.35 (2)	C(25)-C(26)	1.37 (1)
C(26)-C(61)	1.42 (1)	O(5)-C(7)	1.41 (1)
O(6)-C(8)	1.33 (1)	C(52)-C(62)	1.46 (2)
O(1)-O(2)	2.538 (8)	O(1)-O(3)	2.711 (8)
O(2)-O(4)	2.744 (9)	O(3)-O(4)	3.108 (9)
O(1)-N(5)	2.83 (1)	O(2)-N(6)	2.81 (1)
N(5)-N(6)	2.60 (1)		
N(6)-Cu(1)-N(5)	85.8 (4)	N(6)-Cu(1)-O(2)	94.1 (3)
N(6)-Cu(1)-O(1)	167.7 (3)	N(6)-Cu(1)-O(6)	97.8 (3)
N(5)-Cu(1)-O(2)	166.7 (3)	N(5)-Cu(1)-O(1)	95.0 (3)
N(5)-Cu(1)-O(6)	95.8 (3)	O(2)-Cu(1)-O(1)	82.3 (3)
O(2)-Cu(1)-O(6)	97.4 (3)	O(1)-Cu(1)-O(6)	94.3 (3)
O(5)-Fe(1)-O(4)	107.2 (3)	O(5)-Fe(1)-O(1)	87.2 (3)
O(5)-Fe(1)-O(2)	162.3 (3)	O(5)-Fe(1)-O	83.8 (3)
O(4)-Fe(1)-O(1)	163.5 (3)	O(4)-Fe(1)-O(2)	86.9 (3)
O(4)-Fe(1)-O	83.5 (3)	O(1)-Fe(1)-O(2)	77.5 (2)
O(1)-Fe(1)-O	90.3 (3)	O(2)-Fe(1)-O	87.4 (3)
Cu(1)-O(1)-Fe(1)	100.7 (3)	Cu(1)-O(2)-Fe(1)	99.4 (3)

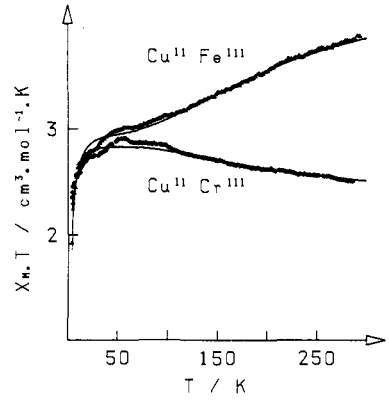

Figure 2. Experimental (▲ or ♦) and theoretical (—) temperature dependencies of $\chi_M T$ for $Cu^{II}Fe^{III}$ and $Cu^{II}Cr^{III}$.

by a bulkier counterion like NO_3^-, the magnetic curve is essentially unchanged; (ii) the magnetic behavior of the $Ni^{II}Fe^{III}$ complex nicely fits the law expected for an uncoupled high-spin Fe^{III} ion with a large axial zero-field splitting.[20] Below 70 K, $\chi_M T$ decreases upon cooling down and tends to a finite value when T approaches zero (see Figure 3). If the spin Hamiltonian is written as

$$\mathcal{H} = g_{Fe}\beta\hat{S}\cdot\vec{H} + D_{Fe}S_z^2 \qquad (1)$$

the g_{Fe} factor assumed to be isotropic and the axial zero-field splitting parameter D_{Fe} are found equal to $g_{Fe} = 1.99$ and $D_{Fe} = 11.8\ cm^{-1}$. In the following, we shall assume that the decrease of $\chi_M T$ on cooling to liquid helium temperature is mainly due to the zero-field splitting of the ground state. This splitting may have several origins, namely the local anisotropy of the Fe^{III} or Cr^{III} ion, the combined effect of the dipole–dipole interaction and

(20) Behere, D. V.; Marathe, V. R.; Mitra, S. *J. Am. Chem. Soc.* **1977**, *99*, 4149–4150.

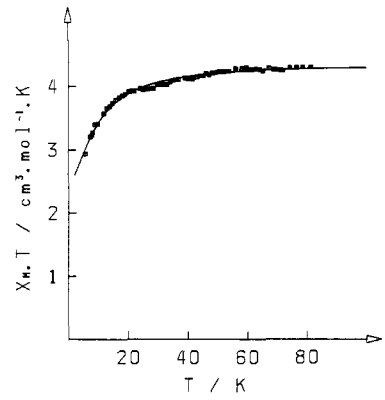

Figure 3. Experimental (□) and theoretical (—) temperature dependencies of $\chi_M T$ for $Ni^{II}Fe^{III}$.

of the anisotropic exchange, and the antisymmetric exchange. It results that the general spin Hamiltonian may be written as follows, where A holds for Cu^{II} and B for Fe^{III} or Cr^{III},

$$\mathcal{H} = \beta H(\mathbf{g}_A\cdot\hat{S}_A + \mathbf{g}_B\cdot\hat{S}_B) + \hat{S}_B\cdot\mathbf{D}_B\cdot\hat{S}_B - J_{AB}\hat{S}_A\cdot\hat{S}_B + \hat{S}_A\cdot\mathbf{D}_{AB}\cdot\hat{S}_B \qquad (2)$$

an expression in which the meaning of all the symbols is now classical.[15,21-23] The antisymmetric exchange of the form $d_{AB}\hat{S}_A \wedge \hat{S}_B$ is zero owing to the C_{2v} molecular symmetry.[24,25] It is clear that it is impossible to extract an unique set of the parameters appearing in (2) from only the magnetic data. Our approach was as follows: (i) Since the interacting ions have no first-order angular momentum, we assumed that the isotropic exchange characterized by J_{AB} was by far the main term in (2). (ii) The local anisotropy of B and the anisotropic exchange together have two effects. At the first order, they split in zero field the two low-lying states; at the second order, they mix the components of the same M_S arising from different states.[15-23] Since the isotropic exchange is assumed to be large, the first-order zero-field splitting of the excited low-lying state is without effect on the magnetic data and the second-order effect may be neglected. Therefore, we shall only take into account the zero-field splitting of the quintet ground state. The zero-field splitting tensor $D_{(2)}$ for this state is related to the parameters of (2) according to the following:[23]

for $Cu^{II}Fe^{III}$

$$D_{(2)} = \frac{4\mathbf{D}_{Fe}}{3} - \frac{\mathbf{D}_{CuFe}}{6} \qquad (3)$$

for $Cu^{II}Cr^{III}$

$$D_{(2)} = \frac{2\mathbf{D}_{Cr} + \mathbf{D}_{CuCr}}{3}$$

(iii) If $\mathbf{g}_a$ is different from $\mathbf{g}_B$, the $\mathbf{g}_{(S)}$ tensors associated with the two states will be also different. Their expressions are as follows:

for $Cu^{II}Fe^{III}$

$$\mathbf{g}_{(2)} = \frac{7g_{Fe} - g_{Cu}}{6}$$

$$\mathbf{g}_{(3)} = \frac{g_{Cu} + 5g_{Fe}}{6}$$

for $Cu^{II}Cr^{III}$

$$\mathbf{g}_{(2)} = \frac{g_{Cu} + 3g_{Cr}}{4}$$

$$\mathbf{g}_{(1)} = \frac{5g_{Cr} + g_{Cu}}{4} \qquad (4)$$

(21) Buluggiu, E. *J. Phys. Chem. Solids* **1980**, *41*, 1175–1180.
(22) Paulson, J. A.; Krost, D. A.; McPherson, G. L.; Rogers, R. D.; Atwood, J. L. *Inorg. Chem.* **1980**, *19*, 2519–2525.
(23) Banci, L.; Bencini, A.; Dei, A.; Gatteschi, D. *Inorg. Chem.* **1981**, *20*, 393–398 and references therein.
(24) Moriya, T. In "Magnetism"; Rado, G. T., Suhl, H., Eds.; Academic Press: New York, 1963; Vol. 1, Chapter 3.
(25) Bencini, A.; Gatteschi, D. *Mol. Phys.* **1982**, *47*, 161–169.

Moreover, the Zeeman term at the second order also couples the components of the same M_S arising from each of the states. This effect, of the order of $(g_A - g_B)^2$, is quite negligible.[15] (iv) Finally, we assumed that all the g tensors were isotropic and that the D tensors were axial with coincident axes. In this framework, the magnetic susceptibilties of $Cu^{II}Fe^{III}$ are expressed according to eq 5 and those of $Cu^{II}Cr^{III}$ according to eq 6.

$$\chi_{\parallel} = \frac{2N\beta^2}{kT}\left[g_{(2)}{}^2\left[\exp\left(\frac{D}{kT}\right) + 4\exp\left(-\frac{2D}{kT}\right)\right] + 14\, g_{(3)}{}^2 \exp\left(\frac{3J}{KT}\right)\right] \Bigg/ \left[\exp\left(\frac{2D}{kT}\right) + 2\exp\left(\frac{D}{KT}\right) + 2\exp\left(-\frac{2D}{kT}\right) + 7\exp\left(\frac{3J}{KT}\right)\right]$$

$$\chi_{\perp} = 2N\beta^2\left[\frac{g_{(2)}{}^2}{3D}\left[9\exp\left(\frac{2D}{kT}\right) - 7\exp\left(\frac{D}{kT}\right) - 2\exp\left(-\frac{2D}{kT}\right)\right] + \frac{14 g_{(3)}{}^2}{kT}\exp\left(\frac{3J}{kT}\right)\right] \Bigg/ \left[\exp\left(\frac{2D}{kT}\right) + 2\exp\left(\frac{D}{kT}\right) + 2\exp\left(-\frac{2D}{kT}\right) + 7\exp\left(\frac{3J}{kT}\right)\right] \quad (5)$$

$$\chi_{\parallel} = \frac{2N\beta^2}{kT}\left[g_{(2)}{}^2\left[\exp\left(\frac{D}{kT}\right) + 4\exp\left(-\frac{2D}{kT}\right)\right] + g_{(1)}{}^2\exp\left(-\frac{2J}{kT}\right)\right] \Bigg/ \left[\exp\left(\frac{2D}{kT}\right) + 2\exp\left(\frac{D}{kT}\right) + 2\exp\left(-\frac{2D}{kT}\right) + 5\exp\left(-\frac{2J}{kT}\right)\right]$$

$$\chi_{\perp} = 2N\beta^2\left[\frac{g_{(2)}{}^2}{3D}\left[9\exp\left(\frac{2D}{kT}\right) - 7\exp\left(\frac{D}{kT}\right) - 2\exp\left(-\frac{2D}{kT}\right)\right] + \frac{g_{(1)}{}^2}{kT}\exp\left(-\frac{2J}{kT}\right)\right] \Bigg/ \left[\exp\left(\frac{2D}{kT}\right) + 2\exp\left(\frac{D}{kT}\right) + 2\exp\left(-\frac{2D}{kT}\right) + 5\exp\left(-\frac{2J}{kT}\right)\right] \quad (6)$$

In (5) and (6), D is the axial zero-field splitting parameter for the $S = 2$ state ($D = {}^3/_2 D_{zz(2)}$).[26] The $g_{(s)}$, J_{AB}, and D parameters were determined by minimizing $R = \sum[(\chi_M T)^{calcd} - (\chi_M T)^{obsd}]^2/\sum[(\chi_M T)^{obsd}]^2$. For each compound, two solutions were found depending on the sign of D. These solutions are for $Cu^{II}Fe^{III}$ $g_{(2)} = 1.99$, $g_{(3)} = 1.97$, $J = -78$ cm^{-1}, $D = 7.8$ cm^{-1}, $R = 8.3 \times 10^{-5}$ or $g_{(2)} = 2.00$, $g_{(3)} = 2.00$, $J = -84$ cm^{-1}, $D = -8.7$ cm^{-1}, $R = 10^{-4}$; for $Cu^{II}Cr^{III}$ $g_{(1)} = 1.98$, $g_{(2)} = 1.95$, $J = 105$ cm^{-1}, $D = 4.5$ cm^{-1}, $R = 1.9 \times 10^{-4}$ or $g_{(1)} = 1.98$, $g_{(2)} = 1.95$, $J = 105$ cm^{-1}, $D = -5$ cm^{-1}, $R = 1.7 \times 10^{-4}$.

For $Cu^{II}Fe^{III}$, the minimum of R is well pronounced whatever the sign of D may be. Therefore, the accuracy on J_{CuFe} is likely to be good. The uncertainty may be estimated at a few wavenumbers. In contrast, for $Cu^{II}Cr^{III}$, the minimum of R is extremely smooth and the uncertainty on J_{CuCr} might be of some tens of wavenumbers. The difficulty to determine accurately the gap between the low-lying states in case of ferromagnetic coupling had already been mentioned.[27] As for the $g_{(S)}$ factors, the accuracy on the determined values is limited by the systematic uncertainties of the magnetic technique, so that it is certainly not possible to check the validity of the relations in (4). The spectra of the low-lying states in $Cu^{II}Fe^{III}$ and $Cu^{II}Cr^{III}$ are schematized in Figure 4. The two complexes are EPR silent in X-band at any temperature down to 4.2 K, which is consistent with a large zero-field splitting of the ground state.

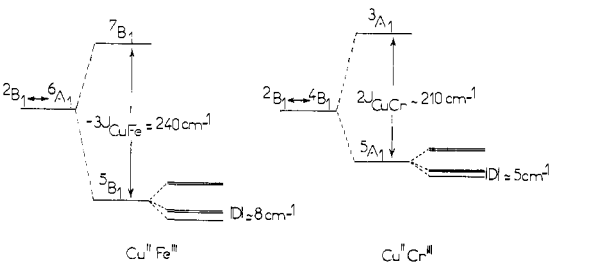

Figure 4. Low lying states in $Cu^{II}Fe^{III}$ and $Cu^{II}Cr^{III}$ (see text).

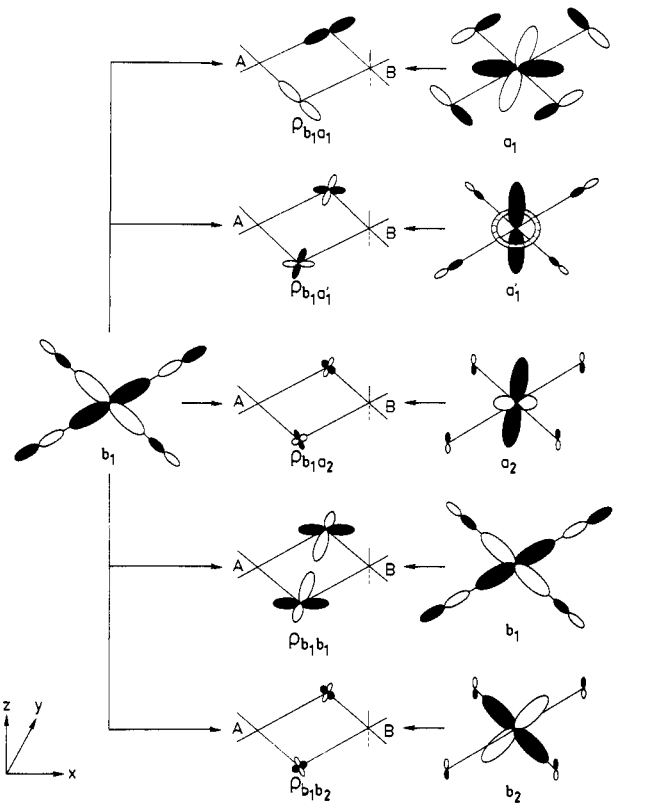

Figure 5. Magnetic orbitals around Cu^{II} (1st column) and around Fe^{III} or Cr^{III} (3rd column), and overlap densities between pairs of magnetic orbitals in $Cu^{II}Fe^{III}$ and $Cu^{II}Cr^{III}$ (see text).

Discussion

The key result of the magnetic study is that in $Cu^{II}Fe^{III}$ the metallic ions interact in an antiferromagnetic manner and in $Cu^{II}Cr^{III}$ they interact in a ferromagnetic manner. It follows that, for both complexes, the ground state is spin quintet. We propose in this section to investigate more thoroughly the mechanism of the interaction. As in the previous section, we assume a C_{2v} symmetry for each metallic site and for the bimetallic complexes in their whole. The unpaired electron around Cu^{II} is described by a magnetic orbital transforming as b_1. The five magnetic orbitals around Fe^{III} transform as $a_1(x^2-y^2$ and $z^2)$, $a_2(yz)$, $b_1(xy)$, and $b_2(xz)$, and the three magnetic orbitals around Cr^{III} transform as $a_1(x^2-y^2)$, $a_2(yz)$, and $b_2(xz)$. These magnetic orbitals are schematized in the first and third columns of Figure 5.

The isotropic exchange parameters may be expressed as sums of components involving pairs of magnetic orbitals according to

$$J_{CuFe} = {}^1/_5\,(J_{b_1a_1} + J_{b_1a'_1} + J_{b_1a_2} + J_{b_1b_1} + J_{b_1b_2}) \quad (7)$$

$$J_{CuCr} = {}^1/_3\,(J_{b_1a_1} + J_{b_1a_2} + J_{b_1b_2}) \quad (8)$$

(26) Abragam, A.; Bleaney, B. In "Electron Paramagnetic Resonance of Transition Ions"; Clarendon Press–Oxford University Press: London, 1969; Chapter 3.

(27) Commarmond, J.; Lehn, J. M.; Plumere, P.; Agnus, Y.; Louis, R.; Weiss, R.; Kahn, O.; Morgenstern-Badarau, I. *J. Am. Chem. Soc.* **1982**, *104*, 6330–6340.

with a_1 and a_1' refering to x^2-y^2 and z^2 type magnetic orbitals, respectively. We proposed an orbital model for describing the exchange interaction in coupled systems.[7,15] In this model, we write down the electrostatic Hamiltonian for the n active electrons ($n = 6$ for $Cu^{II}Fe^{III}$ and $n = 4$ for $Cu^{II}Cr^{III}$) as

$$\mathcal{H} = \sum_{i=1}^{n} h(i) + \sum_{i} \sum_{j>i} \frac{1}{r_{ij}} \tag{9}$$

$h(i)$ is the monoelectronic Hamiltonian acting on the electron i and r_{ij} is the interelectronic distance. Then, we express the wavefunctions associated to the low-lying states as Heitler–London functions constructed from the magnetic orbitals. Expanding the energies of the low-lying states according to the increasing powers of the overlap integrals $S_{\mu\mu}$ between the magnetic orbitals, we obtain for each $J_{\mu\nu}$ component

$$J_{\mu\nu} = 4t_{\mu\nu}S_{\mu\nu} + 2j_{\mu\nu} + \text{terms in } S_{\mu\nu}^2 \ldots \tag{10}$$

with

$$t_{\mu\nu} = \langle \mu_A(i)|h(i) - \frac{\alpha(\mu_A) + \alpha(\mu_B)}{2}|\nu_B(i)\rangle$$

$$\alpha(\mu_A) = \langle \mu_A(i)|h(i)|\mu_A(i)\rangle$$

$$S_{\mu\nu} = \langle \mu_A(i)|\nu_B(i)\rangle$$

$$j_{\mu\nu} = \langle \mu_A(i)\nu_B(j)|r_{ij}^{-1}|\mu_A(j)\nu_B(i)\rangle$$

and $\mu_A(i)$ (or $\nu_B(i)$) denoting a magnetic orbital of symmetry μ (or ν), centered on A (or B). The monoelectronic term $4t_{\mu\nu}S_{\mu\nu}$, proportional to $-S_{\mu\nu}^2$, is negative. It represents the antiferromagnetic contribution to $J_{\mu\nu}$, which is zero for any $\mu \neq \nu$. As for the bielectronic term $2j_{\mu\nu}$, it represents the ferromagnetic contribution to $J_{\mu\nu}$. This term is always positive, whatever the symmetries μ and ν may be.

It is clear that all the $J_{\mu\nu}$ components in (7) and (8), but $J_{b_1b_1}$ are strictly positive owing to the *orthogonality of the magnetic orbitals*. Therefore, the interaction in $Cu^{II}Cr^{III}$ is *purely* ferromagnetic. In contrast, $J_{b_1b_1}$ occurring in (7) has a negative contribution. More generally, when one of the interacting ions has a high-spin d^5 configuration, the strict orthogonality of the magnetic orbitals cannot exist, whatever the symmetry of the system may be.

In a previous paper,[5] we briefly discussed the magnitude of the $J_{\mu\nu}$ components for bimetallic complexes prepared with binucleating ligands of the same symmetry as $[(fsa)_2en]^4$. We propose to detail somewhat this discussion for the pairs $Cu^{II}Fe^{III}$ and $Cu^{II}Cr^{III}$. For that, we schematized the overlap densities $\rho_{\mu\nu}(i) = \mu_A(i)\,\nu_B(i)$ between magnetic orbitals in the second column of Figure 5. We have shown that the magnitude of the interaction may be estimated from such schemes, this being particularly true in case of strict orthogonality of the magnetic orbitals. Each $J_{\mu\nu}$ component may then be written as

$$2\int_{\text{space}} \frac{\rho_{\mu\nu}(i)\rho_{\mu\nu}(j)}{r_{ij}}\, d\tau_i\, d\tau_j$$

of which the magnitude is related to the extremes (positive or negative) of the overlap density $\rho_{\mu\nu}$.

$\rho_{b_1a_1}$, which is maximum in the xy plane, is antisymmetric with regard to the xz mirror plane with two strongly positive lobes around a bridge and two strongly negative lobes around the other bridge. It follows that $J_{b_1a_1}$ is expected to be large. This prediction, in fact, has already been checked experimentally in CuVO[(fsa)$_2$en](CH$_3$OH) where $J_{b_1a_1}$ was found equal to 118 cm^{-1}.[5] $\rho_{b_1a_1'}$ involves a z^2 type magnetic orbital more weakly delocalized toward the bridging oxygen atoms so that the extremes of the overlap density are less pronounced. Thus, $J_{b_1a_1'}$ is expected to be less positive than $J_{b_1a_1}$. $\rho_{b_1a_2}$ and $\rho_{b_1b_2}$ involve magnetic orbitals centered on B, which are very weakly delocalized in a π-manner on the bridges. The xy plane is then a nodal plane. It follows that the two components $J_{b_1a_2}$ and $J_{b_1b_2}$ are expected to be very weak if not negligible. As for $\rho_{b_1b_1}$, it exhibits two positive lobes and two negative lobes around each bridge.[7] The overlap integral $\int_{\text{space}} \rho_{b_1b_1} d\tau$ is very sensitive to small structural changes and may be *accidentally* zero for a very peculiar value of the bridging angles close to 90°. In the binuclear complexes with the $[(fsa)_2en]^{4-}$ ligand, the AOB bridging angles are close to 100°. For these values, the extremes of $\rho_{b_1b_1}$ along the x direction are more pronounced than the extremes of opposite sign along the y direction. $|S_{b_1b_1}|$ may then be large and the antiferromagnetic contribution in $J_{b_1b_1}$ will be predominant. Such a situation was observed in $Cu_2[(fsa)_2en](CH_3OH)$ where $J_{b_1b_1}$ was found equal to −650 cm^{-1}.[28] It can be noticed here that our conclusions remain valid if we take into account the actual C_s symmetry for $Cu^{II}Fe^{III}$. In this case, the $a_1(x^2-y^2)$, $a_1(z^2)$, and $b_2(xz)$ orbitals transform as the a′ irreducible representation of C_s and the $a_2(yz)$ and b_1 (xy) orbitals as a″. This results in a second nonstrictly positive component in J_{CuFe} involving the x^2-y^2 type orbital around Cu^{II} and the yz type orbital around Fe^{III}. However, we have seen above that the corresponding $J_{\mu\nu}$ component was quasi-negligible. To summarize, the main components in (7) and (8) are $J_{b_1a_1}$, which is positive, and $J_{b_1b_1}$, which is negative. Assuming that $J_{b_1a_1}$ has the same value in $Cu^{II}Fe^{III}$ and $Cu^{II}Cr^{III}$, we can deduce from the values of J_{CuFe} and J_{CuCr} $J_{b_1a_1} \sim 300$ cm^{-1} and $J_{b_1b_1} \sim -700$ cm^{-1}. This latter value is close to the one obtained in the $Cu^{II}Cu^{II}$ pair,[28] whereas the former is significantly larger than the one obtained in the $Cu^{II}VO^{II}$ pair.[5] This could be due to the fact that the $a_1(x^2-y^2)$ magnetic orbital around Cr^{III} would be more delocalized toward the bridging oxygen atoms than the $a_1(x^2-y^2)$ magnetic orbital around VO^{II}. Indeed, Cr^{III} is certainly located inside the plane of the macrocycle whereas V^{IV} is pulled out of this plane toward the oxygen atom of the vanadyl group by 0.44 Å.[5] Therefore, the $Cu^{II}<^{X}_{X}>Cr^{III}$ *network could be one of the most efficient to lead to a strong ferromagnetic interaction.*

Concerning the $Cu^{II}Fe^{III}$ pair, the b_1 exchange pathway appears particularly appropriate to propagate a strong antiferromagnetic interaction. The bioinorganic chemists, in the last period, carried out many attempts to synthesize an antiferromagnetically coupled $Cu^{II}Fe^{III}$ complex with the Fe^{III} ion in a porphyrin-type surrounding.[29-32] In this kind of complex, this b_1 pathway does not exist, so that it is not surprising that the goal has not been reached.

Registry No. **3**, 87729-10-0; **4**, 87729-11-1; $Cu^{II}Fe^{III}$, 77322-01-1; $CuH_2[(fsa)_2en]$ sodium salt, 60104-95-2; $FeH_2[(fsa)_2en]Cl(CH_3OH)$ lithium salt, 87760-79-0.

Supplementary Material Available: A listing of structure factor amplitudes and the listing of the magnetic data (18 pages). Ordering information is given on any current masthead page.

(28) Galy, J.; Jaud, J.; Kahn, O.; Tola, P. *Inorg. Chim. Acta* **1979**, *36*, 229-236.
(29) Berry, K. J.; Clark, P. E.; Gunter, M. J.; Murray, K. S. *Nouv. J. Chim.* **1980**, *4*, 581-585.
(30) Gunter, M. J.; Mander, L. N.; Murray, K. S.; Clark, P. E. *J. Am. Chem. Soc.* **1981**, *103*, 6785-6787.
(31) Elliott, C. M.; Akabori, K. *J. Am. Chem. Soc.* **1982**, *104*, 2671-2674.
(32) Dessens, S. E.; Merrill, C. L.; Saxton, R. J.; Ilaria, R. L. Jr.; Lindsey, J. W.; Wilson, L. J. *J. Am. Chem. Soc.* **1982**, *104*, 4357-4361.